MUCOOL Note 159

Compensation of beam-beam interaction in a 50 GeV $\times$ 50 GeV muon collider ring

Eun-San Kim and Moohyun Yoon

Pohang Accelerator Lab., Pohang Univ. of Science of Techlonogy(POSTECH), Korea

Department of Physics, Pohang Univ. of Science of Techlonogy(POSTECH), Korea

August 30, 2000

Abstract

The effect of a beam-beam interaction on the motion of a circulating beam in a 50 GeV$\times$50 GeV muon-collider ring is investigated by weak-strong beam modeling. In the present design of the muon-collider storage ring, the frequency-slippage factor η_1 is approximately -5×10^{-7} so that the synchrotron motion is nearly frozen. This may lead to an increase in the energy spread due to the beam-beam interaction. Through the weak-strong beam modeling, we have investigated the parametric dependencies of the energy spread induced by the beam-beam interaction. We show in this paper that the energy spread due to the beam-beam interaction is large and can be compensated for by employing one rf cavity in the ring with a modest rf voltage.

1 Introduction

It is well known that the beam-beam interaction can limit the performance of collider rings. A particle in a bunch feels a nonlinear force due to electric fields produced by particles in an opposite beam. In the transverse direction, the beam-beam force can induce a tune shift [1]. If the beam size varies significantly within the bunch length, however, the longitudinal effect which the beam energy changes depending on the transverse position should be considered [2]. This is the case for the proposed 50 GeV$\times$50 GeV muon-collider ring [3].

In this paper we present investigations of the beam-beam interaction in a 50 GeV$\times$50 GeV muon-collider ring whose major design characteristics are summarized in Table I. This table shows the three design options of the ring. We note that the muon-collider ring has several remarkable features: (i) the bunch has a large charge ($N = 4\times10^{12}$), (ii) the natural beam energy spread is very small ($\Delta E/E_0 = 0.0012$-3×10^{-5}), (iii) the beta function (β_{IP}) at the interaction point is comparable to the nominal bunch length, (iv) the muon has a lifetime, $\tau_\mu \simeq 1.1$ ms at 50 GeV, corresponding to 1000 turns in a ring with a circumference (C) of 350 meters, and (v) the need to minimize the rf voltage leads to a small slippage factor $\eta_1 = -5 \times 10^{-7}$ and the synchrotron-oscillation period is much longer than the storage time. The small η_1 freezes the longitudinal positions of particles in the beam. Accordingly, the energy variation of a particle in the beam due to the beam-beam interaction accumulates from turn to turn, and may increase the energy spread of the beam. It is necessary to maintain a small energy spread of the beams circulating in a muon-collider ring because this makes it possible for a direct measurement of the resonance cross section of a low-mass Higgs boson.

In order to examine the beam-beam interaction, we resort to a numerical simulation. For the study, a model of the weak-strong beam is employed which is widely used to investigate beam-beam interaction in a collider ring. In the study, the dependence of the bunch length of a beam on the energy spread is included because it is an important consideration since the transverse beam size of the strong beam is a function of the longitudinal position in the interaction region. After we show that the beam energy spread is increased by the beam-beam interaction, we present the parametric dependencies of the energy spread of a beam on various parameters, such as the beam-beam parameter, bunch length, beam size, emittance and betatron function at the interaction point (IP). We then provide a means of controlling the energy spread by showing that the increase in the energy spread can be reduced by adding one rf cavity to the ring with a modest rf voltage. Since the beam intensity decreases due to the muon decay, the rf voltage must vary in time. For completeness, we take all three design options in the muon-collider proposal [3] and apply the simulation to each option separately. In the simulation, both transverse and longitudinal motions are included. The beam-beam interaction in a collider has been treated by many authors: Hirata et al. [2, 4] showed that the energy of a particle in a beam can be changed by the beam-beam interaction caused by the electric field due to particles in an opposite beam. Kim et al. [5] showed that the energy spread of a beam induced by coupling impedances in the 50 GeV$\times$50 GeV muon-collider ring could be compensated for by employing two additional rf cavities. In our study, we consider these works and extend them to explore the compensation of the energy spread induced due to the beam-beam interaction in a muon-collider ring.

The paper is organized as follows. In §2, weak-strong model equations for a round Gaussian beam are presented. Section 3 presents the simulation method and shows various results of applying the simulation to three different designs for the 50 GeV$\times$50 GeV muon-collider ring. Also in §3, it is demonstrated that the energy spread due to the beam-beam interaction can be compensated for by employing one additional rf cavity. Finally, conclusions are given in §4.

2 Equations of Motion

Equations of motion for a particle around a storage ring can be conveniently described by introducing scaled coordinates in transverse and longitudinal phase spaces. With s

denoting the longitudinal coordinate, they are given by

$$Y(s) = \frac{y(s)}{\sigma_{y0}}, \quad Y'(s) = \beta_{IP}\frac{y'(s)}{\sigma_{z0}}, \quad Z(s) = \frac{z(s)}{\sigma_{z0}}, \quad E(s) = \frac{\epsilon(s)}{\sigma_{\epsilon 0}}, \tag{1}$$

where β_{IP} represents the betatron function at the IP and σ_{y0}, σ_{z0} and $\sigma_{\epsilon 0}$ are the nominal rms values at the IP of the transverse beam size, the bunch length and the relative energy spread, respectively. In the above equation, y and y' are the position and the slope of a macroparticle in a weak beam in the transverse direction, respectively, and ϵ is the relative energy deviation from the nominal energy [$\epsilon = (E - E_0)/E_0$]. We use

$$z = s - ct(s), \tag{2}$$

where c is the speed of light, and t is the difference in the arrival time at s between the particle under consideration and the reference particle. Thus, $z(s) > 0$ indicates that the particle arrives at s earlier than the reference particle. Here, we are assuming a round beam, as is the case for a beam in the muon-collider ring. A strong beam is assumed to be at rest at the IP.

The evolutions of these normalized parameters in the ring can be treated separately at the IP and around the arc of the ring. First, at the IP, the change in scaled coordinates due to the beam-beam interaction is given by [2, 4]

$$\begin{aligned}
Y &\to Y - R_1(Z - Z_*)\delta P, \\
Y' &\to Y' + \delta P, \\
Z &\to Z, \\
E &\to E + R_2\delta P(Y' + \frac{\delta P}{2}) - G.
\end{aligned} \tag{3}$$

Here, the beam-beam interaction is modeled by the interaction between a macroparticle in a weak beam and one in a strong beam with several slices. The center of each slice is represented by the longitudinal position z_*. In eq. (3), we have defined

$$\begin{aligned}
\delta P &= 8\pi\xi\frac{n_*}{N_*}\frac{1}{Y + R_1(Z - Z_*)Y'}\left(e^{-A^2} - 1\right), \\
G &= 8\pi\xi\frac{n_*}{N_*}\frac{R_1R_2Z - Z_*}{1 + R_1^2(Z - Z_*)^2}e^{-A^2}, \\
A &= \frac{Y + R_1(Z - Z_*)Y'}{\sqrt{2(1 + R_1^2(Z - Z_*)^2)}}, \\
R_1 &= \frac{\sigma_{z0}}{2\beta_{IP}}, \\
R_2 &= \frac{\epsilon_0}{2\sigma_{\epsilon 0}\beta_{IP}}, \\
Z_* &= \frac{z_*}{\sigma_{z0}}.
\end{aligned} \tag{4}$$

Here, ξ is the nominal beam-beam parameter defined by

$$\xi = \frac{N_* r_e}{4\pi\gamma\epsilon_0}, \tag{5}$$

where ϵ_0 is the transverse nominal emittance of the strong beam, r_e is the classical electron radius and γ is the usual relativistic factor. More detailed discussions of eqs. (3) and (4) can be found in ref. 2.

As mentioned above, the strong beam is divided longitudinally into several slices, and a beam-beam kick given in eq. (3) for each slice is delivered at the barycenter Z_* [6]. Here, Z_* is the longitudinal barycenter of each slice in the strong beam and each barycenter represents n_*/N_* of all particles in the strong beam where N_* and n_* are the numbers of particles in the strong beam and in each slice, respectively.

The transformation in the transverse plane from IP to IP around the ring is simply a rotation:

$$\begin{pmatrix} Y \\ Y' \end{pmatrix} = \begin{pmatrix} \cos 2\pi\nu_y & \sin 2\pi\nu_y \\ -\sin 2\pi\nu_y & \cos 2\pi\nu_y \end{pmatrix} \begin{pmatrix} Y \\ Y' \end{pmatrix}, \tag{6}$$

where ν_y is the betatron tune of a ring.

Neglecting the synchrotron oscillation, as is the case for the muon-collider ring under consideration, the longitudinal phase-space transformation is given by

$$\begin{pmatrix} Z \\ E \end{pmatrix} = \begin{pmatrix} 1 & -\eta_1 \\ 0 & 1 \end{pmatrix} \begin{pmatrix} Z \\ E \end{pmatrix}, \tag{7}$$

where η_1 is the frequency-slippage factor defined by

$$\eta_1 = \alpha - \frac{1}{\gamma^2}. \tag{8}$$

Here, α is the momentum-compaction factor of the ring.

3 Application and Results

It is not difficult to implement eqs. (3), (6), and (7) in a computer program. For the initial parameters of eq. (1), a total number of 20000 macroparticles are distributed with a Gaussian distribution with an average of zero and a root-mean square (rms) value of one. For tracking we take the turn number as an independent variable. Tracking up to 1000 turns is sufficient because it corresponds to the muon lifetime $\tau_\mu \approx 1.1$ ms. In this section, we describe the tracking results for all three designs shown in Table I.

3.1 Design A

3.1.1 Bunch-length effect

As mentioned above, the strong beam was divided into slices to take into account the effect of the initial bunch length on the motion of a beam. To examine this effect, the total number of slices n was varied from one to five. Figure 1(a) shows the resulting normalized rms energy spread as a function of the turn number with different numbers of slices (n=1, 2, 3, 5) in the strong beam. The figure clearly shows that the energy spread depends on n if it is too small. It is seen that the energy spreads for $n = 3$ and $n = 5$ are almost identical, leading to a factor of four increase in the energy spread. Therefore, we take $n = 5$, and this value has been employed in all the simulations below.

Figure 1(b) shows the normalized rms energy spread as a function of the normalized bunch length (σ_{z0}/β_{IP}), where $\beta_{IP} = 14.1$ cm for $n = 1$ and $n = 5$. As the bunch length increases the energy spread increases. The figure shows that as the bunch length increases the number of slices should be sufficiently large to obtain a correct result.

Figure 1(c) describes the normalized rms transverse beam size (σ_y/σ_{y0}) as a function of the turn number up to 1000 orbital turns. The beam-beam parameter ξ, defined in eq. (5), is 0.015 for Design A (see Table I). Figure 1(c) indicates that the beam size increases by only 1%, which is small. From this we can conclude that the beam-beam interaction in a 50 GeV×50 GeV muon-collider ring does not affect the transverse beam size.

3.1.2 Compensation for the energy spread

It was shown in Fig. 1(a) that the energy spread increased due to the beam-beam interaction. It is therefore expected that the longitudinal phase space would be distorted. Figures 2(a) and 2(b) show the beam-phase spaces in the longitudinal direction after one turn in 2(a) and after 1000 turns in 2(b), respectively. In these figures, the horizontal axis denotes the longitudinal position z [see eq. (2)] and the vertical axis represents the relative energy deviation, $\epsilon = (E - E_0)/E_0$, of a particle. Distortion of the phase portrait is apparent in Fig. 2(b).

Figure 2(c) shows the increment of the energy spread of a beam due to the beam-beam interaction in the longitudinal direction after one turn. In order to compensate for the increase in the energy spread, a rf cavity can be utilized in such a way that the rf voltage almost cancels the induced energy spread by applying an opposite kick, as evident in the energy spread due to the additional rf in Fig. 2(c). Since the muon beam decays with time, the magnitude of the applied rf voltage also decreases with time according to

$$V_{rf} = V_0 \; e^{-\frac{NT_0}{\tau_\mu}} \sin(\omega_{rf} t + \phi), \tag{9}$$

where V_0 is the initial amplitude of the applied rf voltage, N is the number of turns, T_0 is the revolution period of a muon beam, τ_μ is the lifetime of a muon particle, and ϕ is the initial rf phase. In eq. (9), the angular frequency ω_{rf} of the rf is determined by the bunch length, and if its value is appropriately chosen together with that of the voltage amplitude V_0, the induced energy spread due to the beam-beam interaction can be minimized.

Figure 2(d) shows the longitudinal beam-phase space after 1000 turns when $f_{rf} = 255$ MHz, V_0 is 16.4 kV and the phase offset $\phi{=}{-}\pi$ (see Table II). Upon comparing this figure with Fig. 2(b), it is clear that in the presence of the rf cavity the induced energy spread due to the beam-beam interaction is significantly reduced. The energy spread due to the beam-beam interaction becomes smaller as the number of turns increases because muons decay with time, and therefore the rf voltage has been reduced in accordance with eq. (9). Figure 2(e) shows the normalized rms energy spread as a function of turn number with the applied rf voltage. This figure is compared with Fig. 1(a), which shows the energy spread in the absence of the rf. We see that with the rf the normalized rms energy spread is increased by only 3% after 1000 turns. Figures 2(d) and 2(e) clearly show that the energy spread due to the beam-beam interaction in the 50 GeV$\times$50 GeV muon-collider ring can be compensated for by one rf cavity with a low rf voltage.

3.1.3 Dependence on the betatron tune

In obtaining Figs. 1 and 2, the betatron tune $\nu_y = 6.239$ has been used which is the design tune for the muon-collider ring. In order to examine the dependence of the beam size and the energy spread on the tune, the tune value has been scanned and the resulting beam size and energy spread as a function of the tune value are shown in Figs. 3(a) and 3(b), respectively. In these figures, the rf voltage has been applied. The figures show similar behaviors; both the beam size and the energy spread increase significantly near $2\nu_y \sim integers$. Away from these resonances, the beam size and the energy spread are not sensitive to the tune. However, since we are neglecting sextupoles and high-order multipoles in the ring, the beam size and the energy spread are expected to be affected near $m\nu_x + n\nu_y = p$ resonances, where m, n and p are integers.

3.1.4 Dependence on beam-beam parameter

It is also expected that the transverse beam size and the energy spread are affected by the beam-beam parameter ξ. Figure 4 shows the variation of these two parameters as a function of ξ. This figure indicates that the transverse beam size remains approximately constant and increases by about 2% between $\xi = 0.015$ and $\xi = 0.075$. On the other hand, it is seen that the energy spread is a strong function of ξ. To obtain the figure, the rf voltage was applied with the parameters given above.

3.2 Design B

3.2.1 Compensation for the energy spread

Figures 5(a) and 5(b) show the beam-phase spaces for Design B (see Table I) after one turn and after 1000 turns without an rf cavity. Similar to Design A, the phase space after 1000 turns is distorted by the beam-beam interaction, as can be seen in Fig. 5(b).

Figure 5(c) shows the increment of the energy spread due to the beam-beam interaction in the longitudinal direction after one turn. The increment of the energy spread due to the application of an rf voltage is also shown. In this case, the applied rf voltage is 28.2 kV and the rf frequency f_{rf} is 260 MHz. The phase offset ϕ is $-\pi$ rad. With these parameters, the longitudinal phase space after 1000 turns is shown in Fig. 5(d). This figure, when compared with Fig. 5(b), indicates that the addition of an rf cavity improves the energy spread induced by the beam-beam interaction.

Figure 5(e) shows the normalized rms energy spread as a function of turn number. The energy spread both with and without the rf cavity is shown. It is evident that the rms energy spread in the presence of the rf cavity is increased by only 1.5% after 1000 turns. In the absence of the rf cavity the rms energy spread is increased by more than 90%. Therefore, the advantage of introducing an rf cavity is clearly demonstrated in this case as well. Table II lists the parameters of the rf cavity.

3.3 Design C

3.3.1 The energy spread

Figures 6(a) and 6(b) show the beam-phase spaces for Design C after one turn in (a) and after 1000 turns in (b) in the absence of the rf voltage. It is evident that the initial energy spread does not change noticeably after 1000 turns. This is because the nominal relative rms energy spread in Design C, $\sigma_{\epsilon 0} = 0.0012$, is already large, so that the contribution of the beam-beam interaction is only a fraction of it. Therefore, in the case of Design C, the addition of an rf cavity will not be effective in reducing the energy spread due to the beam-beam interaction.

4 Conclusions

The effect of the beam-beam interaction in a 50 GeV$\times$50 GeV muon-collider ring has been investigated with a multiparticle tracking simulation. Three types of lattice designs have been considered. The simulation demonstrated the necessity of including the bunch-length effect. It was shown that the transverse beam size was not affected significantly by the beam-beam interaction. On the other hand, the energy spread due to the beam-beam interaction caused a large beam-energy spread, but the growth of the energy spread could be controlled by employing an additional rf cavity with a modest rf voltage.

References

[1] H. Mais and C. Mari: CERN 94-01 (1994) 499.

[2] K. Hirata, H. Moshammaer and F. Ruggiero: Part. Accel. **40** (1993) 205.

[3] C.M. Ankenbrandt, et al.: Phys. Rev. Special Topics: Accelerators and Beams **2** (1999) 081001.

[4] K. Hirata, H. Moshammaer and F. Ruggiero: CERN SL-AP/90-02, 1990.

[5] E.-S. Kim, A.M. Sessler and J.S. Wurtele: Phys. Rev. Special Topics: Accelerators and Beams **2** (1999) 051001.

[6] S. Krishnagopal and R. Siemann: Phys. Rev. D **41** (1990) 2312.

Table 1: Major parameters for three designs of the proposed 50 GeV×50 GeV muon-collider ring.

	Design A	Design B	Design C
Number of μ/bunch	4×10^{12}	4×10^{12}	4×10^{12}
Luminosity	$10^{31}/\mathrm{cm}^2\mathrm{s}$	$2.2\times10^{31}/\mathrm{cm}^2\mathrm{s}$	$1.2\times10^{32}/\mathrm{cm}^2\mathrm{s}$
Relative rms energy spread	0.00003	0.0001	0.0012
Beta function at IP	14.1 cm	9.4 cm	4.1 cm
Rms bunch length	14.1 cm	9.4 cm	4.1 cm
Beam-beam parameter	0.015	0.022	0.051
Rms beam size at IP	294 μm	196 μm	86 μm
Circumference	350 m	350 m	350 m

Table 2: RF cavity parameters for compensation of energy spreads due to beam-beam interaction.

	Design A	Design B	Design C
RF Frequency f_{rf}	255 MHz	260 MHz	None
Initial RF Voltage V_{rf}	16.4 kV	28.2 kV	None
Phase offset ϕ	$-\pi$ radian	$-\pi$ radian	None

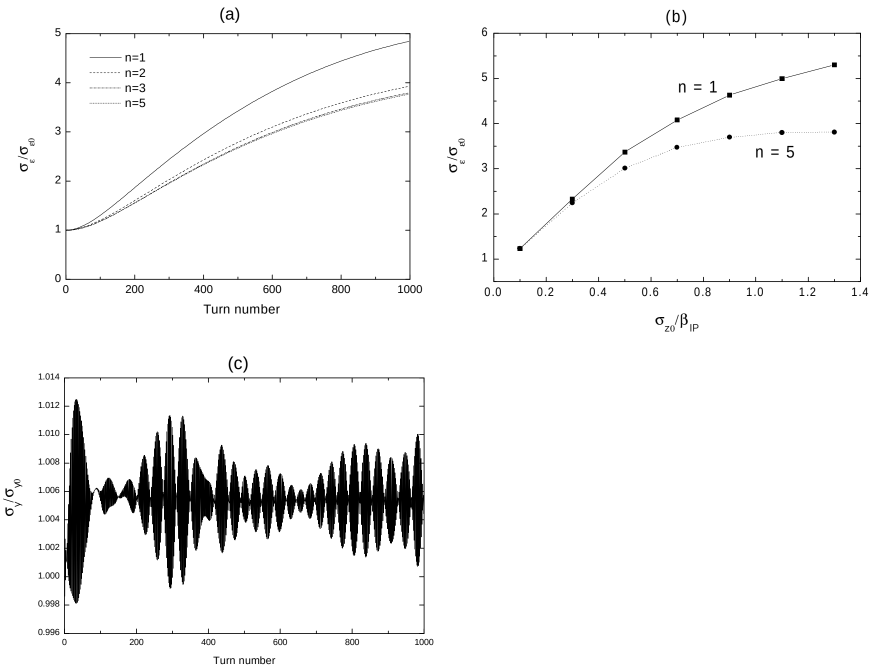

Fig. 1

Figure 1: (a) Normalized rms energy spread ($\sigma_\epsilon/\sigma_{\epsilon 0}$) as a function of turn number and number of slices (n): $n = 1$, $n = 2$, $n = 3$ and $n = 5$ are shown from top to bottom. (b) Normalized rms energy spread as a function of the normalized nominal bunch length (σ_{z0}/β_{IP}) at the interaction point. The solid curve is for $n = 1$ and the dotted curve shows for $n = 5$. (c) Normalized rms transverse beam size (σ_y/σ_{y0}) as a function of turn number. It is seen that the effect of beam-beam interaction is negligible to the growth of the transverse beam size. In each figures, ν_y=6.239, ξ=0.015 and $\sigma_{yIP} = 294\ \mu m$.

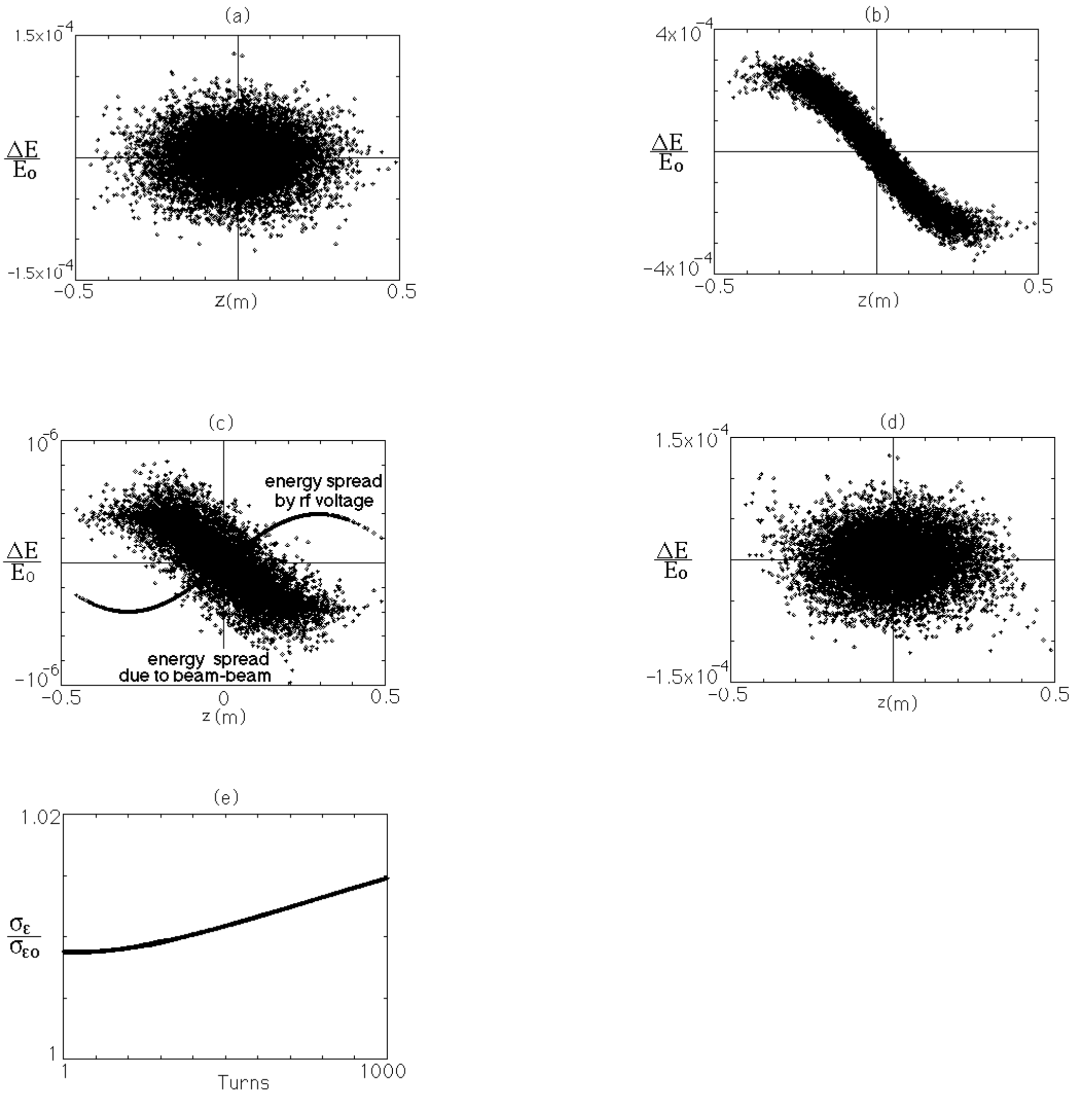

Figure 2: Longitudinal phase space distribution (a) after one turn and (b) after 1000 turns. (c) increments of the energy spread due to the beam-beam interaction after one turn. Energy spread by one RF voltage after 1 turn is also shown. (d) longitudinal phase space after 1000 turns when the energy spread due to the beam-beam interaction is compensated by one RF voltage. (e) Normalized rms energy spread as a function of turn number with an RF voltage applied. In each figure, ν_y=6.239, ξ=0.015 and $\sigma_{yIP} = 294\ \mu m$. The number of slices are five.

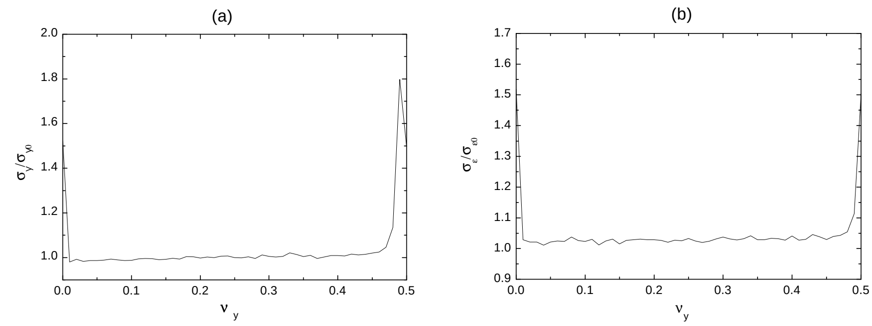

Fig. 3

Figure 3: Tune dependence on (a) the normalized rms beam size (σ_y/σ_0) and (b) the normalized rms energy spread $(\sigma_\epsilon/\sigma_{\epsilon o})$ after 1000 turns. $\xi = 0.015$ and $\sigma_{yIP} = 294\ \mu m$. The number of slices are $n = 5$.

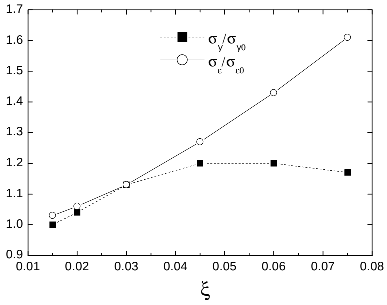

Figure 4: Beam-beam parameter (ξ) dependence on the scaled rms beam size (solid curve) and the scaled rms energy spread (dashed curve) after 1000 turns. $\sigma_{yIP} = 294\ \mu m$. ν_y=6.239. The number of slices are $n = 5$.

Fig. 4

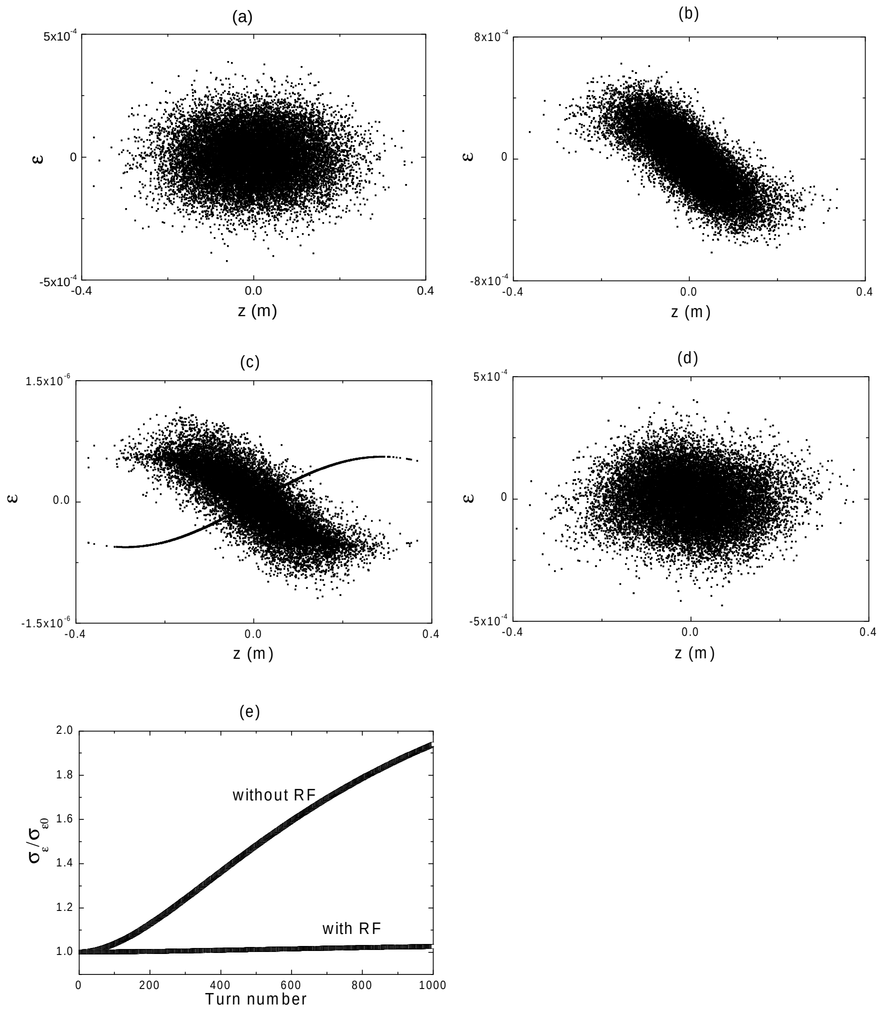

Fig. 5

Figure 5: Longitudinal phase space distribution (a) after one turn and (b) after 1000 turns. (c) increments of the energy spread due to the beam-beam interaction after one turn. Energy spread by one RF voltage after one turn is also shown. (d) longitudinal phase space after 1000 turns when the energy spread due to the beam-beam interaction is compensated by one RF voltage. (e) normalized rms energy spread as a function of turn number with an RF voltage applied. In each figure, ν_y=6.239, ξ=0.022 and $\sigma_{yIP} = 196\ \mu m$. The number of slices are five.

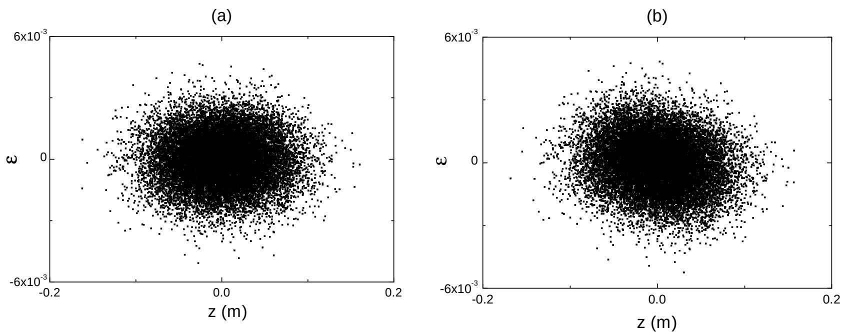

Figure 6: Beam phase space distribution (a) after one turn and (b) after 1000 turns. In each figure, ν_y=6.239, ξ=0.051 and $\sigma_{yIP} = 86\ \mu m$. The number of slices $n = 5$ are used.

Fig. 6